

ARTICLE OPEN

Flexible high energy density zinc-ion batteries enabled by binder-free MnO₂/reduced graphene oxide electrodeYuan Huang¹, Jiuwei Liu¹, Qiyao Huang², Zijian Zheng², Pritesh Hiralal³, Fulin Zheng³, Dilek Ozgit³, Sikai Su⁴, Shuming Chen⁴, Ping-Heng Tan⁵, Shengdong Zhang¹ and Hang Zhou¹ 

We demonstrate a rechargeable zinc-ion battery with high energy density and cyclability using MnO₂ and reduced graphene oxide (MnO₂/rGO) electrode. The flexible and binder free electrode, with high MnO₂ mass ratio (80 wt% of MnO₂), is fabricated using vacuum filtration without any additional additives other than rGO. Compared to batteries with conventional MnO₂ electrodes, the Zn–MnO₂/rGO battery shows a significant enhanced capacity (332.2 mAh g⁻¹ at 0.3 A g⁻¹), improved rate capability (172.3 mAh g⁻¹ at 6 A g⁻¹) and cyclability. The capacity retention remains 96% after 500 charge/discharge cycles at 6 A g⁻¹. The high MnO₂ mass ratio makes MnO₂/rGO electrode advantageous when the capacity is normalized to the whole electrode, particularly at high rates. The calculated gravimetric energy density of Zn–MnO₂/rGO battery is 33.17 W h kg⁻¹, which is comparable to the existing commercial lead-acid batteries (30–40 W h kg⁻¹). Furthermore, the discharge profile and capacity of our Zn–MnO₂/rGO battery shows no deterioration during bending test, indicating good flexibility. As a result, zinc-ion battery is believed to be a promising technology for powering next generation flexible electronics.

npj Flexible Electronics (2018)2:21; doi:10.1038/s41528-018-0034-0

INTRODUCTION

There is an increasing demand of high safety, high energy density and low cost energy storage device for wearable or flexible electronics. In this aspect, aqueous zinc-ion batteries (ZIBs) have received incremental attention because of their high safety, abundance of Zn source, and environmental friendliness.^{1–5} MnO₂ is a most common low cost cathode material for ZIBs, which provides high capacity, large voltage window (~2 V) and high output voltage (~1.3 V).^{6–8} While the exact reaction mechanism of MnO₂ in ZIBs remains to be explored, it is generally believed that, similar to other types of ion batteries, the Zn-insertion process into MnO₂ is an important step. In this regard, the phase, powder structure and conductivity of MnO₂ are critical for realizing high energy density ZIBs. Nonetheless, MnO₂ suffers from low electronic conductivity (10⁻⁵–10⁻⁶ S cm⁻¹), which leads to unsatisfactory performance, such as low capacity and low rate capability.^{7–9} Many attempts have been made to tackle this problem, including doping of MnO₂,⁷ coating conductive surface layer⁶ and adding conductive additives,^{9,10} etc. Among them, adding conductive materials (with mass ratio ranging from 20 to 33%) to the MnO₂ cathode has been frequently employed in preparing the MnO₂-based cathode,^{6,9–11} due to its ease of fabrication. Examples include depositing poly(3,4-ethylenedioxythiophene) (PEDOT) layer on the surface of MnO₂ and forming MnO₂/acid-treated carbon nanotube nanocomposites.^{6,9} These electrodes exhibited high reversible capacity (310 mA h g⁻¹ at 1.11 A g⁻¹ (see ref. ⁶)), fast charging and discharging capability (143.3 mA h g⁻¹ at 7.43 A g⁻¹ (see ref. ⁶)), and good cycling stability

(100 mA h g⁻¹ at 5 A g⁻¹ up to 500 cycles⁹). Usually, binders (such as polytetrafluoroethylene (PTFE), polyvinylidene fluoride (PVDF), or carboxymethyl cellulose with mass ratio around 10%) are required to construct a workable cell.^{9–11} This is done at the expense of reduced active material content. Therefore, finding efficient additives that enhance the electronic conductivity of MnO₂, while at the same time minimizing the content of both additives and binders, become an attractive approach for achieving high mass loading of active material in the battery.

There are several requirements for screening the optimum conducting additives for MnO₂. First of all, the additives should not react with electrolyte or cathode materials. Second, the adopted materials should be light weight, and also possess high surface area. Ideally, the additives should be able to wrap up the MnO₂ nanopowders and form a percolating conducting network. Finally, the additives should also facilitate ion transportation in the composite matrix. Taking all these into account, reduced graphene oxide (rGO), due to its light weight, excellent electrical conductivity and high specific surface area, is considered as an ideal additive candidate for the MnO₂ electrode. The benefits of rGO additives in battery electrodes have been previously demonstrated in lithium-ion batteries and supercapacitors.^{12–14} The MnO₂/rGO composite structure with high specific surface area and mesopores has been noted to be favorable for improving both the main pseudocapacitance of MnO₂ and the electric double-layer capacitance of rGO.¹⁴ In addition, the use of nanostructured MnO₂/rGO composites as a Faradic electrode can also improve the electrical conductivity of the electrode.

¹Shenzhen Key Lab of Thin Film Transistor and Advanced Display, Peking University Shenzhen Graduate School, Peking University, 518055 Shenzhen, China; ²Laboratory for Advanced Interfacial Materials and Devices, Institute of Textiles and Clothing, The Hong Kong Polytechnic University, Hong Kong S. A. R., China; ³Zinergy UK Ltd., Future Business Centre, Cambridge CB4 2HY, UK; ⁴Department of Electrical and Electronic Engineering, Southern University of Science and Technology, 518055 Shenzhen, China and ⁵State Key Laboratory of Super Lattices and Microstructures, Institute of Semiconductors, Chinese Academy of Sciences, 100083 Beijing, China

Correspondence: Hang Zhou (zhouh81@pkusz.edu.cn)

These authors contributed equally: Yuan Huang, Jiuwei Liu.

Received: 14 March 2018 Revised: 21 June 2018 Accepted: 4 July 2018

Published online: 30 July 2018

Similarly to supercapacitors, the electrodes for the lithium ion batteries application required easy transportation of electrons through the highly conductive rGO channels. MnO₂/rGO composites with high specific surface area afford more active sites for lithium redox reactions and better access to Li ions, leading to increased capacity and improved rate capability.¹² Moreover, the mesopores in the composite accommodates the volume expansion of MnO₂ during the process of charge/discharge, resulting in superior cycling stability.¹² Here, we adopt vacuum filtration, a simple experimental method, to deposit MnO₂ nanosheets and rGO sheets onto the carbon cloth. The vacuum filtration method is a simple fabrication process to prepare MnO₂/rGO electrode. In fact, vacuum filtration is known to deposit densely packed active materials. It is capable of producing uniform deposits with an intimate interface between active materials (MnO₂/rGO in the present case) and current collector (carbon cloth in this case). It has the additional advantage of producing samples free of binders and other additives, which increases the packing density of the active material. In this manner, we have obtained a flexible, binder free MnO₂/rGO cathode with high MnO₂ mass ratio (80 wt% of MnO₂). ZIBs with MnO₂/rGO electrode (Fig. 1) demonstrate enhanced capacity, improved rate capability and cycling performance, when compared to a control sample with the conventional MnO₂ electrodes. More importantly, the high MnO₂ mass ratio makes MnO₂/rGO electrode advantageous when the capacity is normalized to the whole electrode, particularly at high rates.

RESULTS AND DISCUSSION

General characterizations of the MnO₂ and MnO₂/rGO samples

The MnO₂ samples were synthesized by a hydrothermal method. XRD result of MnO₂ samples is shown in Fig. 2a. All Bragg peaks can be indexed to the crystalline phase of α -MnO₂ (JCPDS: 44-0141). The SEM image shown in Fig. 2b discloses the nanosheet structure of α -MnO₂, with lengths/width in micrometer scale and thickness in less than tens of nanometers. The MnO₂ nanosheets were believed to provide high surface area as well, and were intentionally grown for this study. Fig. 2c gives the typical TEM image of the α -MnO₂ sample, showing a crumpled surface. The α -MnO₂ is further revealed in the HRTEM (the inset of Fig. 2c) with an interlayer spacing between the MnO₂ sheets estimated to be 0.69 nm, which can be ascribed to the (110)

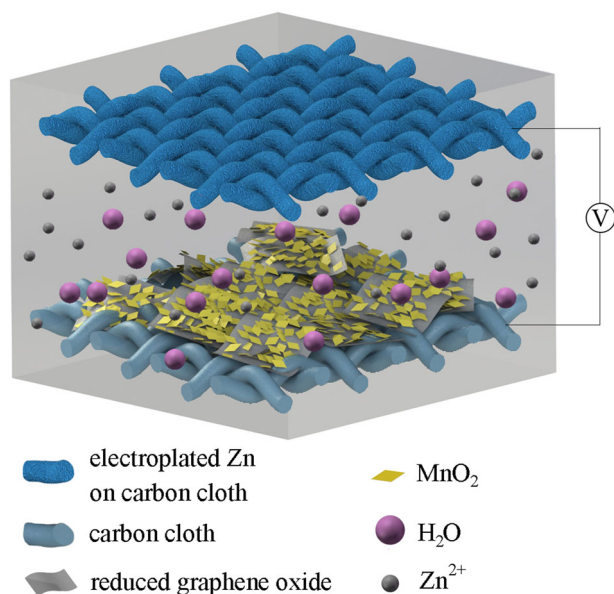


Fig. 1 Schematics of the Zn–MnO₂/rGO battery

planes of α -MnO₂. The α -MnO₂ is featuring for its (2 × 2) + (1 × 1) tunnel structure,¹ which would facilitate Zn insertion. It is highly possible that the Zn-insertion/extraction occurs in the [2 × 2] tunnels of the α -MnO₂ since the geometric dimension of the tunnels (size ~4.6 Å) in α -MnO₂ is sufficiently wide to accommodate guest Zn²⁺ (size ~0.74 Å) ion-insertion/extraction.¹⁵

The MnO₂/rGO electrodes were prepared using a vacuum filtration method (Fig. 2d). Fig. 2e–j shows the representative structural characterization results taken from the MnO₂/rGO sample. The SEM image shown in Fig. 2e provides a general view of the morphology. The MnO₂/rGO sample presents a loose structure that comprises numerous highly wrinkled MnO₂ nanosheets with the size of 100–200 nm, and rGO nanosheets with slightly larger dimensions. The overall thickness of the MnO₂/rGO film lying over carbon cloth is ~130 μm, measured from the cross-sectional SEM image (Fig. 2f). EDX elemental mapping gives the spatial distribution of the compositional elements (Fig. 2g–j). It confirms the existence of MnO₂ nanosheets and the rGO sheets. The structure of rGO has been examined using Raman spectroscopy, which data displays the degree of graphitization of carbon. As shown in Fig. S1, Raman spectrum of rGO shows two typical peaks of graphene, centered at 1351 and 1598 cm⁻¹, corresponding to its D and G bands.¹⁶ The D band is attributed to defects and disordered portions of carbon (sp³), whereas the G band is indicative of ordered graphitic crystallites of carbon (sp²). As a comparison, additional peaks centered at 555 and 645 cm⁻¹ are observed in the Raman spectrum of the MnO₂/rGO sample. They are related to the ν_3 (Mn–O) stretching vibrations and ν_2 (Mn–O) symmetric stretching vibrations of MnO₆ groups, respectively.¹⁷ The BET surface area of MnO₂/rGO sample is 201.6 vs. 63.744 m² g⁻¹ for conventional MnO₂. The nitrogen adsorption–desorption isotherms of MnO₂/rGO sample (Fig. S2) appear to be type IV curves with the H3 hysteresis loops that can be linked to slit-shaped pores.

Comparison between MnO₂/rGO and conventional MnO₂ electrodes

The electrochemical properties of MnO₂/rGO electrode are fairly sensitive to the amount of rGO. Insufficient amount of rGO additives would not be able to enhance conductivity of the mixture, whereas overloading of rGO additives would reduce the capacity of the electrode. In experiments, specific capacities of the MnO₂/rGO electrodes with different MnO₂/rGO ratios (15, 20, and 25 wt% rGO) have been investigated, and the results are presented in Fig. S3. The optimum MnO₂/rGO ratio has been identified to be 8:2 in experiments. The electrochemical properties of the MnO₂/rGO electrodes with a mass ratio of 8:2 have been compared to those of the conventional MnO₂ electrode (70 wt% MnO₂ nanosheets, 20 wt% Super P, and 10 wt% PVDF binder). To make the samples more comparable, the same mass ratio of conductive additive was introduced to the conventional MnO₂ electrode. Electroplated Zn on carbon cloth was used as counter electrode. More details of the electrodes preparation can be found in the Experimental section. The morphology of electroplated Zn on carbon cloth is presented in Fig. S4.

Fig. 3a shows cyclic voltammogram (CV) of the MnO₂/rGO and conventional MnO₂ electrodes at a scan rate of 0.2 mV s⁻¹ in voltage range of 1.0–1.9 V vs. Zn²⁺/Zn. For conventional MnO₂ cathode, two separated reversible redox peaks (reduction peaks: 1.26 and 1.39 V, oxidation peak: 1.55 and 1.60 V) can be clearly observed, corresponding to a two-step reaction. The reaction mechanism for MnO₂ has been reported previously that the MnO₂ cathode experiences a consequent H⁺ and Zn²⁺ insertion/extraction process during the discharging/charging.¹⁸ The MnO₂/rGO sample shows similar oxidation/reduction peaks during the anodic/cathodic scan, indicating that the rGO additive did not affect the redox reactions in the MnO₂ electrode. Nevertheless, the

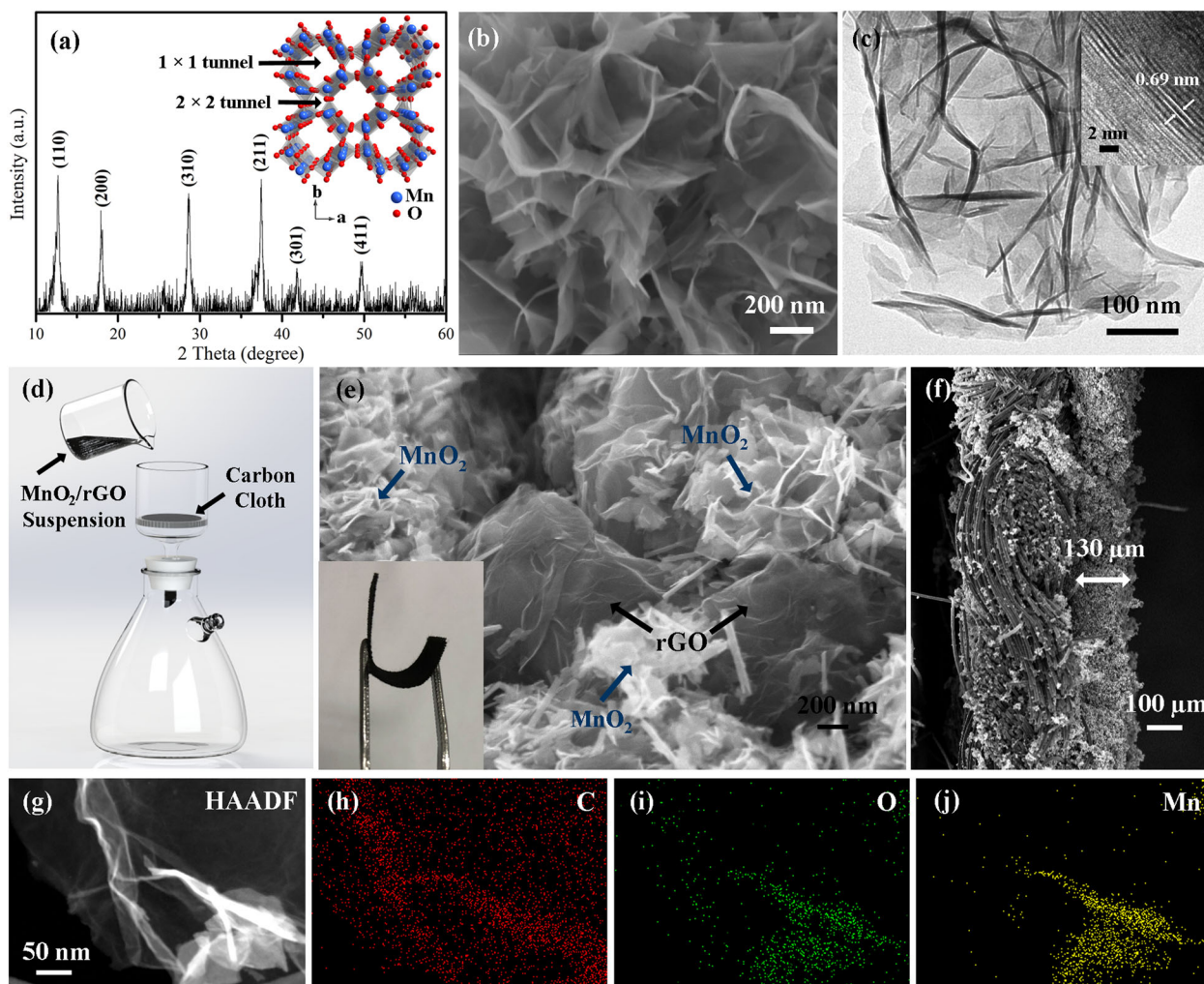


Fig. 2 Preparation and morphology of MnO_2/rGO sample. **a** XRD spectrum of MnO_2 sample. Inset in **a**: crystallographic structure of $\alpha\text{-MnO}_2$. **b** SEM image taken from the MnO_2 sample. **c** TEM image taken from the MnO_2 sample. Inset in **c**: high resolution TEM image of MnO_2 nanosheets. **d** Schematic diagram of the vacuum filtration on carbon cloth for preparing MnO_2/rGO electrodes. **e** SEM image and the photographs (the inset) of the MnO_2/rGO sample on carbon cloth. **f** The cross-sectional SEM image of MnO_2/rGO on carbon cloth. **g** High angle annular dark field (HAADF) image taken from part of the MnO_2/rGO sample. **h–j** EDX elemental maps taken from the same region shown in **g**

magnitudes of their current density of peaks are different. The MnO_2/rGO electrodes show much higher peaks than the conventional MnO_2 electrodes, indicating its higher capacity than the conventional MnO_2 electrodes. Figure 3b and Fig. S5 compare the charging and discharging profiles of the samples at the current density of 0.3 A g^{-1} . Both batteries present two similar discharge plateaus, which are attributed to consequent H^+ and Zn^{2+} insertion process.¹⁸ However, the discharging capacity of the MnO_2/rGO electrodes at 0.3 A g^{-1} is significant higher ($\sim 332.2 \text{ mAh g}^{-1}$) than that of the conventional MnO_2 electrode ($\sim 259.1 \text{ mAh g}^{-1}$). This result is consistent with the CV profiles in Fig. 3a. Figure 3c shows comparison of the rate performance of the MnO_2/rGO and conventional MnO_2 electrodes. It is obvious that the MnO_2/rGO electrode exhibits superior rate capability when compared to the conventional MnO_2 electrode. For example, the MnO_2/rGO sample can deliver discharging capacity of $\sim 332.2 \text{ mAh g}^{-1}$ at low rate of 0.3 A g^{-1} . A little decrease in the discharging capacity is observed when the rate is increased to 0.6 A g^{-1} , and is kept at ~ 227.5 and $\sim 172.3 \text{ mAh g}^{-1}$ at further rate increase to 3, and 6 A g^{-1} , respectively. As a comparison, the conventional MnO_2 electrodes exhibits much lower discharge capacity, that is, $\sim 259.1 \text{ mAh g}^{-1}$ even at low discharge rate of

0.3 A g^{-1} , and further drops to $\sim 82.7 \text{ mAh g}^{-1}$ at 6 A g^{-1} . The capacity of pure rGO electrode is also studied to check whether rGO contributes to the capacity of MnO_2/rGO electrode. As shown in Fig. S6, in contrast, the pure rGO electrode exhibits extremely low capacity, indicating the negligible contribution to overall capacity of the examined MnO_2/rGO electrodes by employing rGO as the conductive additive.

Similar to the specific capacity, the capacity retention would improve when rGO is incorporated. It is worth to note that the binder free MnO_2/rGO maintains much higher capacity retention when discharged at large current density. As shown in Fig. 3c, the MnO_2/rGO sample shows $\sim 51.9\%$ capacity retention (at 6 A g^{-1}) of the first discharging capacity at 0.3 A g^{-1} , which is about twice higher than that of the conventional MnO_2 sample ($\sim 31.9\%$ at 6 A g^{-1}).

To obtain a better understanding on the difference between the ZIB samples with different electrodes, the electrochemical impedance spectroscopy (EIS) measurements were carried out on the ZIBs after charging to $\sim 1.9 \text{ V}$ vs. Zn^{2+}/Zn . The corresponding Nyquist plots (dot) and fitting results (line) are shown in Fig. 3d. An appropriate equivalent circuit model (inset in Fig. 3d) is established to fit the Nyquist curves. The electrical parameters

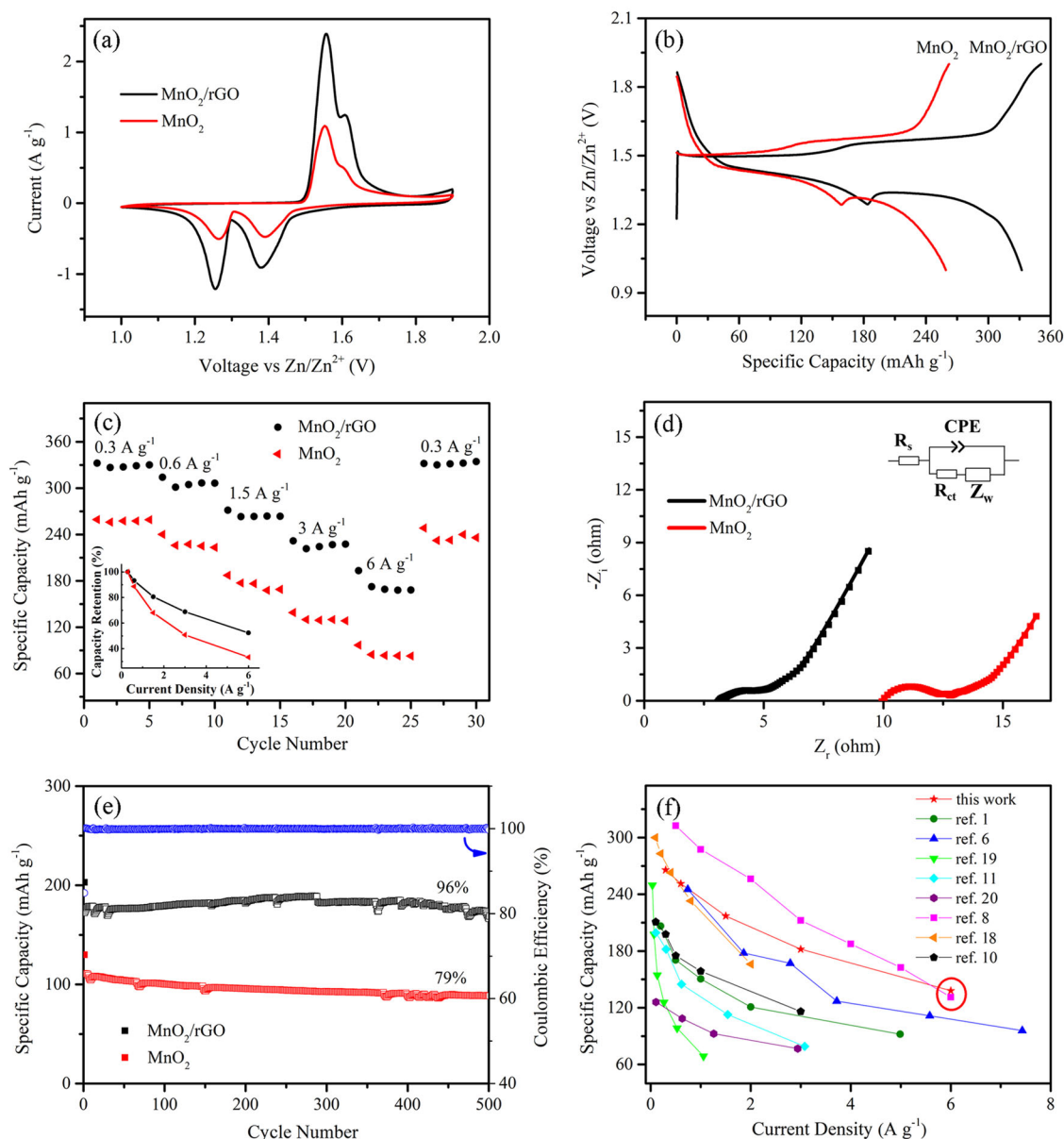


Fig. 3 Electrochemical performance of MnO_2/rGO and conventional MnO_2 electrodes. **a** Cyclic voltammogram of the MnO_2/rGO and conventional MnO_2 electrodes at a scan rate of 0.2 mV s^{-1} in 1.0–1.9 V vs. Zn^{2+}/Zn . **b** Comparison of the charging and discharging profiles of the samples at the current density of 0.3 A g^{-1} . **c** Specific capacities (normalized over the mass of MnO_2) of the samples at various current density. Inset in Fig. **c**: comparison of the specific capacity retention of the samples. **d** Nyquist plots of the samples after charging to $\sim 1.9 \text{ V}$ vs. Zn^{2+}/Zn . **e** Cycling stability of the samples (MnO_2/rGO and conventional MnO_2 electrodes) cycled at 6.0 A g^{-1} and corresponding Coulombic efficiency of MnO_2/rGO electrode. **f** A summary graph of the specific capacity (based on the total mass of the whole electrode material, including MnO_2 , additive and binder) of our MnO_2/rGO electrode and other reported MnO_2 -based electrodes for ZIB at different current densities

(e.g., R_s : solution resistance; R_{ct} : charge-transfer resistance; Z_w : Warburg diffusion process) in this model can be calculated, as shown in Table S1†. The charge-transfer resistance of MnO_2/rGO sample is 1.2Ω , which is lower than that of conventional MnO_2 sample (3.1Ω). The large R_s difference of MnO_2/rGO and conventional MnO_2 electrodes can be ascribed to the reduction of internal resistance due to the rGO additive, which is conductive and reduces the resistance contribution of the electrode. MnO_2 by itself is a very poor conductor, and the addition of binder (PVDF) in conventional MnO_2 electrode also increases the internal resistance of the electrodes. Overall, the binder-free structure of MnO_2/rGO electrode leads to the reduction of internal resistance.

The cycling performance of the MnO_2/rGO sample is also improved especially at high rates when compared to conventional MnO_2 samples (Fig. 3e). More than 96% of its initial capacity and high Coulombic efficiency ($>99.7\%$) still remained even the cyclic number extended to 500 cycles at high current density of 6.0 A g^{-1} , indicating the excellent cycling stability of the MnO_2/rGO sample. As a comparison, the capacity retention of the conventional MnO_2 sample at 6.0 A g^{-1} (after 500 cycles) is 79%. To examine the structure stability of the MnO_2/rGO cathode and electroplated Zn anode, the morphological changes were characterized after the 300 cycles. For the cathode, as shown in Fig. S4c, MnO_2/rGO structure after cycling remains nearly unchanged as compared to

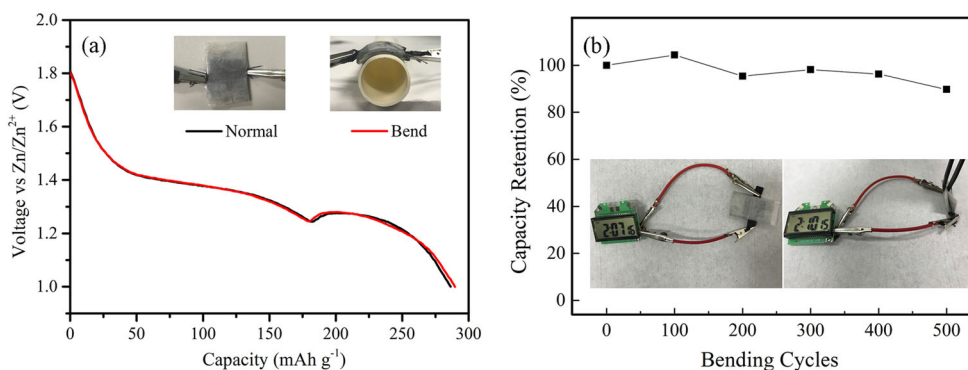


Fig. 4 Flexible Zn–MnO₂/rGO battery. **a** Discharge curves under normal and bending conditions. **b** The bending test of the flexible Zn–MnO₂/rGO battery for 500 cycles. Inset shows the flexible Zn–MnO₂/rGO battery powers a timer under normal and 180 degrees of bending conditions

the morphology of the pristine MnO₂/rGO electrode. The experimental results suggest good structural stability of the MnO₂/rGO electrode. For the anode, SEM images of Zn anode (Fig. S4d) after 300 cycles show freestanding Zn nanosheets homogeneously grown on the carbon fiber. No needle-like dendrites were observed in the SEM image of Zn anode after cycling.

On the basis of the results above, the incorporation of rGO in MnO₂-based electrodes improves the electrochemical properties of the cathode, featuring high specific capacity, superior cycling performance at high charge/discharge rate. This enhancement is probably ascribed to the formation of conductive pathways for electron transport during the charging/discharging process, as evidenced in decreased charge transfer resistance (Fig. 3d). This highly electronic network can improve the conductivity of MnO₂, which contributes to the excellent electrochemical performance of the MnO₂/rGO electrode. Moreover, the rGO additives leads to a higher specific surface area of the MnO₂/rGO electrode (201.578 m² g⁻¹ for MnO₂/rGO electrode vs. 63.744 m² g⁻¹ for conventional MnO₂ electrode), which increases the contact area between electrode and electrolyte, therefore facilitating the Zn²⁺ insertion process.

The vacuum filtration method is a simple fabrication process to prepare MnO₂/rGO electrode. When compared with reported filtration methods in the literature using conventional filtration membranes (e.g., filter papers), the use of carbon cloth as filtration membranes allows the one-step fabrication of the electrode, as it avoids the transfer process. Moreover, this method is capable of producing samples free of binders and other additives, which increases the packing density of the MnO₂. The advantage of high packing density of the active material in the MnO₂/rGO electrode can be further justified when the capacity is normalized to the whole electrode. As shown in Fig. 3f, when the specific capacity is normalized over on the total mass of the whole electrode material (including MnO₂, additive and binders), the MnO₂/rGO electrode is comparable to the best reported results, presenting the highest specific capacity at high current density (~138 mA h g⁻¹ at 6 A g⁻¹) among the MnO₂-based electrodes for ZIBs reported to date.^{1,6,8,10,11,18–20} We also calculated the specific capacity based on the whole weight of MnO₂/rGO electrode (including carbon cloth). The specific capacity based on the whole electrode (including carbon cloth) is around 44 mAh g⁻¹ at 0.3 A g⁻¹.

The energy and power densities of our Zn–MnO₂/rGO battery are shown in Fig. S7. The maximum energy density is 456.2 W h kg⁻¹ and peak power density is 7.9 kW kg⁻¹. Taking the total mass of the cell (including active materials, additive, binders and current collectors of both anode and cathode) into consideration, the gravimetric energy density of Zn–MnO₂/rGO battery is 33.17 W h kg⁻¹, which is much higher than that of typical commercial

supercapacitors (5–10 W h kg⁻¹) and comparable to the existing commercial lead-acid batteries (30–40 W h kg⁻¹).^{21,22}

Flexible Zn–MnO₂/rGO battery

For wearable applications, energy storage devices are required to be highly flexible. Herein, we tested the flexibility of the Zn–MnO₂/rGO battery by bending the devices around a radius of 1 cm. The batteries can be bent without deteriorating the discharge profile and capacity (Fig. 4a). The highest bending angle of Zn–MnO₂/rGO battery approaches 180°, as shown in Fig. 4b. The flexibility of Zn–MnO₂/rGO battery was tested by bending a Zn–MnO₂/rGO battery for 500 times with a bending angle of 180°. Ninety percent capacity was retained after 500 times bending cycles (Fig. 4b). These observations demonstrate a good mechanical stability of the electrodes. Moreover, the battery successfully powered a quantum-dot light emitting diodes display, a timer and light-emitting diodes under bending condition, demonstrating its promising potential in personalized wearable electronics (Fig. 4b and Fig. S8).

CONCLUSION

In summary, MnO₂/rGO electrode has been successfully fabricated by a vacuum filtration process, which results in a flexible and binder/additive free cathode for ZIBs. When compared to conventional MnO₂ cell, the MnO₂/rGO cathode shows largely enhanced capacity, excellent rate capability and cycling stability. The presence of rGO effectively enhances the charge transport and increase the specific surface area in the electrode, resulting in large capacity and outstanding rate performance. The results strengthen our hypothesis that rGO is ideally suited for good ionic transport into the electrode and electronic transport from the electrode. Furthermore, the removal of an extra component (the binder) should help reduce production cost and ease manufacture of the electrode paste. Our work demonstrates that the MnO₂/rGO electrodes are one of the most attractive cathodes in zinc storage applications. With the excellent device performance, the ease of fabrication, such Zn–MnO₂/rGO batteries are very promising for use as wearable energy storage devices.

METHODS

Preparation of MnO₂/rGO electrode

The MnO₂ nanosheets were synthesized by a hydrothermal method.²³ 0.1264 g KMnO₄ and 0.0428 g (NH₄)₂SO₄ were homogeneously mixed with 40 mL distilled water. The solution was then poured into a Teflon-lined reactor and was subjected to hydrothermal condition at 140 °C for 24 h. Then, the resulting powder was filtered and washed with plenty of distilled water. Finally, the filtered powder was dried in a vacuum oven at 60 °C for

2 h, following an annealing process at 300 °C for 1 h under air atmosphere. The mass loading of the MnO₂ is ~3 mg cm⁻².

The MnO₂/rGO electrodes were prepared using a vacuum filtration method. Twelve milligram MnO₂ nanosheets and 3 mg rGO were dispersed in 3 mL isopropyl alcohol (IPA) by sonication for 2 h, and then mixed to form a uniform suspension. The suspension was filtered through carbon cloth on the top of a filter paper (with a pore size of 450 nm), via vacuum filtration. Finally, the electrode was dried in a vacuum oven at 60 °C for 2 h.

Structure and morphology characterization

The morphologies and elemental analyses were characterized by a field-emission scanning electron microscope (FESEM, Zeiss SUPRA-55). Transmission electron microscopy (TEM) measurements were also carried out with a Tecnai F20 (FEI) microscope operating at 200 kV. The crystallinity and phases of the samples were examined by X-ray diffraction (XRD, D8 Advance). Raman analysis was performed using a Raman spectrometer (Jobin-Yvon Horiba Evolution) with an Ar⁺ laser at 514 nm. A Brunauer–Emmett–Teller (BET) analyser (Micromeritics Tristar II 3020 v1.03 analyzer) was used to study the surface area by nitrogen gas absorption–desorption.

Electrochemical characterization

The electrochemical properties of the MnO₂/rGO electrode were characterized by using electroplated Zn on carbon cloth as a counter electrode. Zn was deposited on carbon cloth by an electrodeposition method.⁶ The electrolyte used was 2 M ZnSO₄ with 0.1 M MnSO₄ as an additive in H₂O. A conventional MnO₂ electrode is composed of 70 wt% MnO₂ nanosheet, 20 wt% Super P, and 10 wt% PVDF, which were coated on carbon cloth. CV was measured on an electrochemical station (CHI660, Shanghai CH Instrument Co., Ltd.) with potential range from 1.0 to 1.9 V vs. Zn²⁺/Zn. The assembled cells were cycled at a constant current mode using a CT2001A multichannel battery test system (Wuhan Kingnuo Electronic Co., Ltd.). The EIS of the batteries was measured on an electrochemical station (CHI660, Shanghai CH Instrument Co., Ltd.) under an alternating current (AC) stimulus with 5 mV amplitude. The frequency ranges from 100 kHz to 0.1 Hz.

Data availability

All data generated or analysed during this study are included in this published article and its supplementary information files.

ACKNOWLEDGEMENTS

This work is supported by the China Postdoctoral Science Foundation funded project (2017M620517), the Shenzhen Science and Technology Innovation Committee (No. JCYJ20170818090257257, JCYJ20170412150411676 and JCYJ20160229122349365), and The Hong Kong Polytechnic University (1-YW0Z). Dr. Y. Huang acknowledges the financial support of the Zheng Hanming Visiting Scholar Award from International Teochew Doctors Association.

AUTHOR CONTRIBUTIONS

Y.H. and J.L. contributed equally to this work. Y.H., H.Z. and Z.Z. conceived the idea. Y. H., J.L., and Q.H. designed the work. S.S. and S.C. carried out the fabrication of quantum-dot light emitting diodes display. P.-H.T. provided Raman data. J.L. provided the rest of the experimental data. F.Z., D.O., and Z.S. participate in the data analysis and interpretation. Y.H. drafted the article. H.Z., P.H., and Z.Z. revised the article.

ADDITIONAL INFORMATION

Supplementary information accompanies the paper on the *npj Flexible Electronics* website (<https://doi.org/10.1038/s41528-018-0034-0>).

Competing interests: The authors declare no competing interests.

Publisher's note: Springer Nature remains neutral with regard to jurisdictional claims in published maps and institutional affiliations.

REFERENCES

- Zhang, N. et al. Rechargeable aqueous zinc-manganese dioxide batteries with high energy and power densities. *Nat. Commun.* **8**, 405 (2017).
- Zhang, N. et al. Cation-deficient spinel ZnMn₂O₄ cathode in Zn(CF₃SO₃)₂ electrolyte for rechargeable aqueous Zn-ion battery. *J. Am. Chem. Soc.* **138**, 12894–12901 (2016).
- He, P. et al. Layered VS₂ nanosheet-based aqueous Zn ion battery cathode. *Adv. Energy Mater.* **7**, 1601920 (2017).
- Xia, C. et al. Rechargeable aqueous zinc-ion battery based on porous framework zinc pyrovanadate intercalation cathode. *Adv. Mater.* **30**, 1705580 (2017).
- He, P. et al. Sodium ion stabilized vanadium oxide nanowire cathode for high-performance zinc-ion batteries. *Adv. Energy Mater.* **8**, 1702463 (2018).
- Zeng, Y. et al. Achieving ultrahigh energy density and long durability in a flexible rechargeable quasi-solid-state Zn-MnO₂ battery. *Adv. Mater.* **29**, 1700274 (2017).
- Alfaruqi, M. H. et al. Ambient redox synthesis of vanadium-doped manganese dioxide nanoparticles and their enhanced zinc storage properties. *Appl. Surf. Sci.* **404**, 435–442 (2017).
- Qiu, W. et al. High-performance flexible quasi-solid-state Zn-MnO₂ battery based on MnO₂ nanorod arrays coated 3D porous nitrogen-doped carbon cloth. *J. Mater. Chem. A* **5**, 14838–14846 (2017).
- Xu, D. et al. Preparation and characterization of MnO₂/acid-treated CNT nanocomposites for energy storage with zinc ions. *Electrochim. Acta* **133**, 254–261 (2014).
- Wu, B. et al. Graphene scroll-coated α-MnO₂ nanowires as high-performance cathode materials for aqueous Zn-ion battery. *Small* **14**, 1703850 (2018).
- Pan, H. et al. Reversible aqueous zinc/manganese oxide energy storage from conversion reactions. *Nat. Energy* **1**, 16039 (2016).
- Lee, S.-W. et al. Superior electrochemical properties of manganese dioxide/reduced graphene oxide nanocomposites as anode materials for high-performance lithium ion batteries. *J. Power Sources* **312**, 207–215 (2016).
- Chang, J. et al. Asymmetric supercapacitors based on graphene/MnO₂ nanospheres and graphene/MoO₃ nanosheets with high energy density. *Adv. Funct. Mater.* **23**, 5074–5083 (2013).
- Wu, Z.-S. et al. High-energy MnO₂ nanowire/graphene and graphene asymmetric electrochemical capacitors. *ACS Nano* **4**, 5835–5842 (2010).
- Alfaruqi, M. H. et al. Enhanced reversible divalent zinc storage in a structurally stable α-MnO₂ nanorod electrode. *J. Power Sources* **288**, 320–327 (2015).
- Huang, Y., Liu, H., Gong, L., Hou, Y. & Li, Q. A simple route to improve rate performance of LiFePO₄/reduced graphene oxide composite cathode by adding Mg²⁺ via mechanical mixing. *J. Power Sources* **347**, 29–36 (2017).
- Yang, B. et al. A three dimensional Pt nanodendrite/graphene/MnO₂ nanoflower modified electrode for the sensitive and selective detection of dopamine. *J. Mater. Chem. B* **3**, 7440–7448 (2015).
- Sun, W. et al. Zn/MnO₂ battery chemistry with H⁺ and Zn²⁺ coinserion. *J. Am. Chem. Soc.* **139**, 9775–9778 (2017).
- Islam, S. et al. Facile synthesis and the exploration of the zinc storage mechanism of β-MnO₂ nanorods with exposed (101) planes as a novel cathode material for high performance eco-friendly zinc-ion batteries. *J. Mater. Chem. A* **5**, 23299–23309 (2017).
- Xu, C. et al. Energetic zinc ion chemistry: the rechargeable zinc ion battery. *Angew. Chem. Int. Ed.* **51**, 933–935 (2012).
- Li, K., Liu, J., Huang, Y., Bu, F. & Xu, Y. Integration of ultrathin graphene/polyaniline composite nanosheets with a robust 3D graphene framework for highly flexible all-solid-state supercapacitors with superior energy density and exceptional cycling stability. *J. Mater. Chem. A* **5**, 5466–5474 (2017).
- Tateishi, H. et al. Graphene oxide lead battery. *ECS Electrochem. Lett.* **3**, A19–A21 (2014).
- Lee, B. et al. Elucidating the intercalation mechanism of zinc ions into α-MnO₂ for rechargeable zinc batteries. *Chem. Commun.* **51**, 9265–9268 (2015).



Open Access This article is licensed under a Creative Commons Attribution 4.0 International License, which permits use, sharing, adaptation, distribution and reproduction in any medium or format, as long as you give appropriate credit to the original author(s) and the source, provide a link to the Creative Commons license, and indicate if changes were made. The images or other third party material in this article are included in the article's Creative Commons license, unless indicated otherwise in a credit line to the material. If material is not included in the article's Creative Commons license and your intended use is not permitted by statutory regulation or exceeds the permitted use, you will need to obtain permission directly from the copyright holder. To view a copy of this license, visit <http://creativecommons.org/licenses/by/4.0/>.

© The Author(s) 2018